Supplemental Data

The Peroxin Loss-of-Function Mutation *abstinence by mutual consent* Disrupts Male-Female Gametophyte Recognition

Aurélien Boisson-Dernier, Sabine Frietsch, Tae-Houn Kim, Marie B. Dizon, and Julian I. Schroeder

Supplemental Results and Discussion

amc/+ Complementation by Introduction of a Wild-Type Copy of At3g07560

To determine whether the disruption of At3g07560 was indeed responsible for the observed phenotypes in *amc*/+, we transformed *amc*/+ plants with a 4.4 Kb long genomic construct containing only the wild-type At3g07560 gene and its flanking sequences (see Supplemental Experimental Procedures). In 13 out of 16 T1 lines containing the T-DNA insertion in *APM2/AMC*, a wild-type-like full seed set was restored. To further confirm the complementation, from one of those 13 lines, we selected a homozygous T2 plant for the genomic construct and heterozygous for the T-DNA insertion in At3g07560. Within the progeny of this plant, PCR-based genotyping of 48 T3 individuals resulted in the identification of 12 wild-type, 22 heterozygous, and 14 homozygous individuals for the T-DNA insertion in At3g07560 at an expected 1:2:1 ratio for complementation ($\chi^2 = 0.5$, $0.9 > p > 0.7$). In addition, the percentage of Kanamycin-resistant seedlings was restored to 77.5% (252 Kan^R seedlings out of 325), which is not significantly different from the 75% expected for the segregation of a single dominant marker ($\chi^2 = 1.12$, $0.6 > p > 0.5$). Furthermore, within the progeny of a T3 plant homozygous for both the T-DNA in At3g07560 and the genomic construct, all the seedlings were Kanamycin resistant ($n > 300$), as expected. Together, these results show that introduction of a wild-type copy of *APM2/AMC* rescued the seed-set phenotype, as well as the absence of homozygotes and the distorted segregation observed for *amc*/+ plants. Therefore, the T-DNA insertion in At3g07560 is indeed triggering the *amc*/+ phenotypes, and *amc*/+ is a loss-of-function mutation.

APM2/AMC Exhibits Low Level of Similarity with PEX13 but Does Not Have a SH3 Domain

Database analyses indicated that *AMC* is a single gene in *Arabidopsis thaliana* but has orthologs in *Musa acuminata*, *Medicago truncatula*, and *Oryza sativa* (Figure S1A). APM2/AMC sequence analysis with protein-analysis software (blastp2 at the ExPASy proteomic server) [S1] predicted a low level of similarity to the SH3-domain-containing peroxin PEX13 from various organisms (15.9% identity with PEX13 from *Saccharomyces cerevisiae*; Figure S1B). All PEX13 proteins identified thus far possess an SH3 domain that mediates protein-protein interaction and retains high sequence similarity among residues involved in ligand binding and a perfectly conserved secondary structure with five stranded β barrels [S2, S3]. The homology between APM2/AMC and PEX13 is almost nonexistent within the SH3 domain (Figures S1B and S1C). Furthermore, two different programs for protein-domain recognition, ScanProsite (http://www.expasy.org/tools/scanprosite/) [S4] and Pfam (http://pfam.janelia.org/) [S5] did not recognize any SH3 domain within the APM2/AMC sequence, whereas they did for PEX13 proteins from many organisms, as well as for the *Arabidopsis* SH3-domain-containing protein 1 (AtSH3P1; NP_174429). Finally, the SSpro protein secondary structure prediction program (http://www.ics.uci.edu/~baldig/scratch/index.html) [S6] could not detect a single stranded β barrel within the putative SH3-domain sequence for APM2/AMC (Figure S1D) [S7]. Therefore, we propose that APM2/AMC has no SH3 domain and might not be a direct ortholog of PEX13.

The *amc* Mutation Disrupts Processes before Embryo Formation

To investigate whether the *amc* mutation triggers embryonic lethality, we analyzed developing seeds in heterozygous *amc*/+ siliques by using Nomarski optics 54 hr after manual pollination. *amc*/+ siliques contained approximately 78% of normal young seeds with globular embryos ($n = 316$ out of 406; Figure S2A, left panel) as wild-type siliques (data not shown). The remaining ovules ($n = 92$ out of 406) showed no sign of either embryo or free-nuclear endosperm formation (Figure S2A, right panel). They were easily distinguishable from normal young seeds because they were smaller and started senescing. In addition, the micropylar ends of these ovules often contained tangled structures (Figure S2A, right panel, white arrows) that were not observed in unfertilized wild-type mature ovules (data not shown). Because no obvious signs of fertilization were observed in the senescing ovules, it is very likely that the *amc* mutation triggers defects in fertilization or in events that precede fertilization rather than embryonic lethality.

To determine whether these unfertilized ovules were targeted by pollen tubes, 72 hr after manual pollination, siliques of heterozygous *amc*/+ plants were treated with Aniline blue, which stains the callose of pollen-tube cell walls. This analysis revealed that PTs reached the micropyles of all of the small senescing ovules ($n > 300$; Figure S2B, top) as frequently as they did for normal developing young seeds (Figure S2B, bottom). Together, these data suggest that the incomplete seed set observed for the *amc*/+ siliques is the result of ovules normally targeted by PTs that remain unfertilized.

Delayed Synergid Cell Degeneration in the *amc/+* Mutant

So that the synergid cell's status in the *amc*/+ mutant could be investigated, homozygous transgenic wild-type and *amc*/+ lines expressing the YFP-containing cameleon D3 reporter driven by the synergid-specific *MYB98* promoter were generated [S8]. Before fertilization, about 90% ($n > 300$) of the mature female gametophytes of both wild-type and *amc*/+ pistils showed a strong YFP fluorescence restricted to the synergid

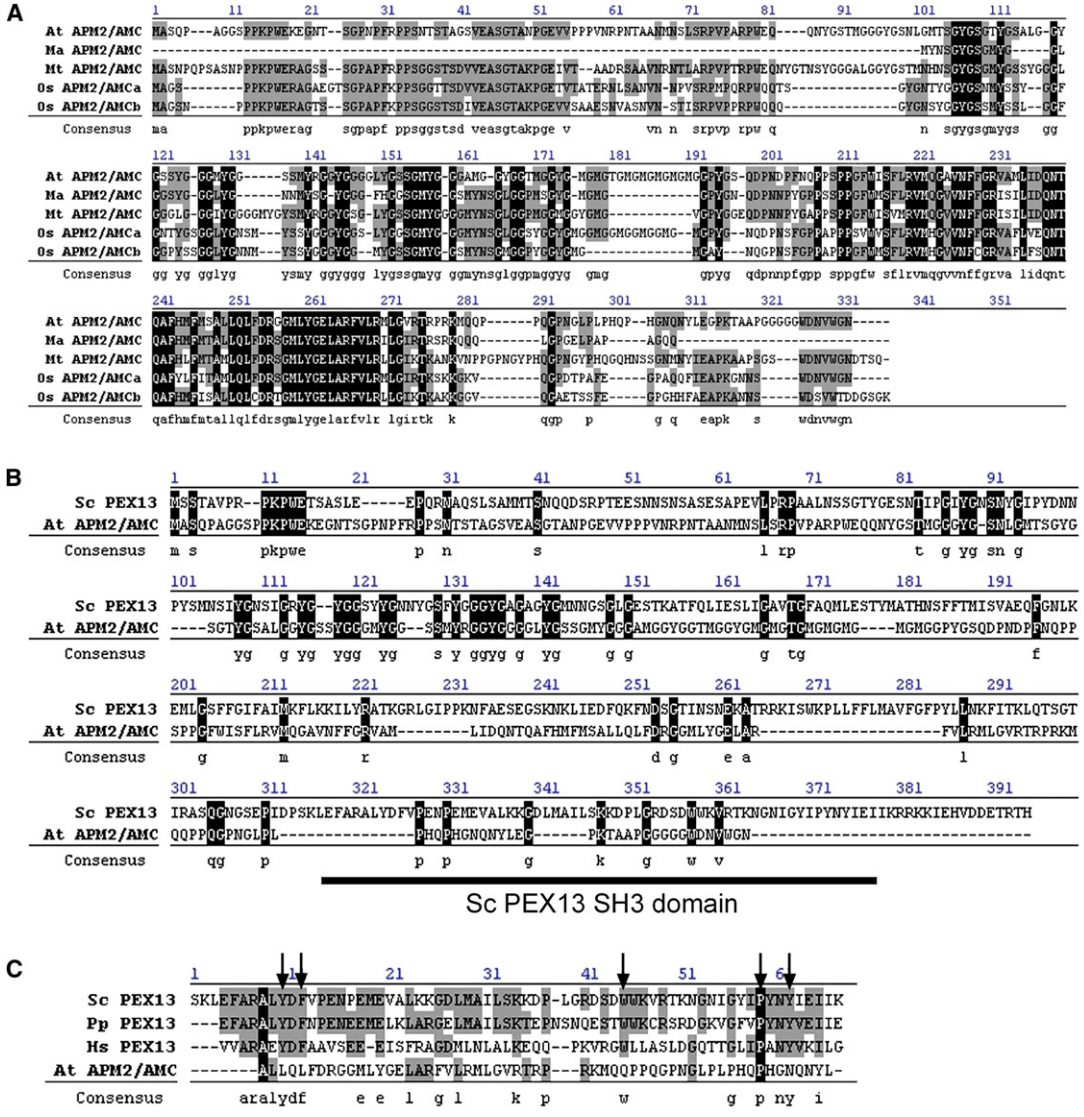
A
At APM2/AMC
Ma APM2/AMC
Mt APM2/AMC
Os APM2/AMCa
Os APM2/AMCb
Consensus
B
Sc PEX13
At APM2/AMC
Consensus
Sc PEX13 SH3 domain
C
Sc PEX13
Pp PEX13
Hs PEX13
At APM2/AMC
Consensus
D
Sc PEX13
seq: SKLEFARALYDFVPENPEMEVALKKGDLMAILSKKDPLGRDSDWWKVRTKNGNIGYIPYNYIEIIK
pred: CCCEEEEEEECCCCCCCCCCCCCCCCCEEEEEECCCCCCCCCCCEEEECCCCCEEEECCCHEEEEC
Pp PEX13
seq: ----EFARALYDFNPENEEMELKLARGELMAILSKTEPNSNQESTWWKCRSRDGKVGFVPYNYVEIIE
pred: ----CEEEEEEECCCCCCCCCCCCCCCCCEEEEEECCCCCCCCCCCEEEEECCCCCEEEECCCEEEEEC
Hs PEX13
seq: ---VVARAEYDFAAVSEEEISFRAGDMLNLALKEQQPKVRGWLLASLDGQTTGLIPANYVKILG
pred: ---CEEEEEECCCCCCCCCCCCCCCCCEEEEECCCCCCCCCCCCEEEECCCCCEEEEECCCEEEECC
At APM2/AMC
seq: -------ALLQLFDRGGMLYGELARFVLRMLGVRTRPRKMQQPPQGPNGLPLPHQPHGNQNYL
pred: -------CHHHHHCCCCCHHHHHHHHHHHHHCCCCCCCCCCCCCCCCCCCCCCCCCCCCCC

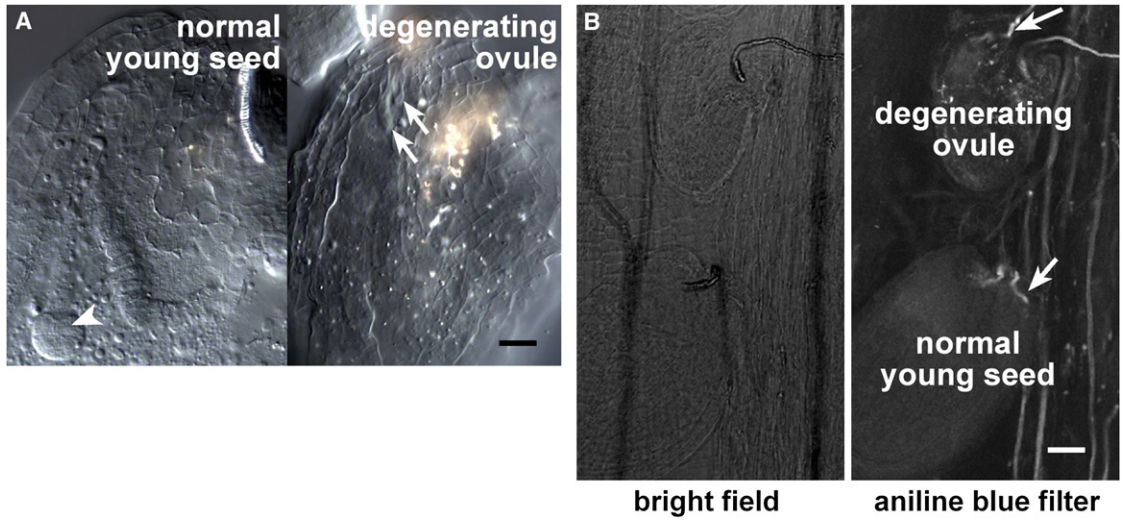

Figure S2. The *amc* Mutation Disrupts Processes before Embryo Formation

(A) Structure of cleared *amc*/+ ovules 54 hr after manual self-pollination as observed with Nomarski optics. Siliques of *amc*/+ plants contained both normal young seeds with globular embryos (left panel, white arrowhead) and degenerating ovules with tangled structures in the micropylar end of the embryo sac (right panel, white arrows). There was no sign of fertilization in the degenerating ovules. The scale bar represents 30 μm.

(B) Visualization of ovule targeting by pollen tubes 72 hr after manual self-pollination in *amc*/+ siliques with Aniline blue staining. Micropyles of both normal young seeds (bottom) and degenerating ovules (top) are targeted by pollen tubes (white arrows). Bright field is used in the left panel, and Aniline blue filter is used in the right panel. The scale bar represents 50 μm.

cells (Figure S3A). No difference could be observed for the pMYB98-D3 expression pattern and for the overall structure between wild-type and *amc*/+ mature FGs (data not shown). Therefore, synergid cells of *amc*/+ appeared to be normally specified and differentiated.

For the visualization of both synergid cells and pollen tubes during fertilization, pACA9-DsRED-expressing pollen of wild-type and *amc*/+ homozygous lines were deposited on pistils of wild-type and *amc*/+ plants expressing the pMYB98-D3 fusion. In the siliques from wild-type crosses, pollen-tube discharge (magenta color) was typically associated with a pMYB98-D3 signal (green channel) that started to diffuse in the embryo sac, as previously reported for synergid cell degeneration (Figure S3B) [S8]. In contrast, during an *amc* mutant interaction, the pMYB98-D3 signal was still restricted to the synergids, whereas the pollen tube branched and appeared to grow around and past the synergids (Figure S3C). This suggests that during an *amc* mutant interaction, the mutant pollen tube does not penetrate the mutant synergid cells, although they are in close contact and synergid degeneration is delayed.

Genetic Interaction between FER and APM2/AMC Pathways

Pollen from *amc*/+ (Col-0) plants were deposited on *fer*/+ (Ler) pistils, and the resulting F1 Kanamycin-resistant plants were genotyped for both the T-DNA insertion in *APM2/AMC* and the Ds element in At3g51470 linked to the *feronia* mutation [S9]. In this F1 population, *amc*/+ plants (Ler × Col-0) exhibited siliques filled to 77.3% with nonaborted ovules (Table S3), similar to the original *amc*/+ plants in the Col-0 background ($\chi^2 = 0.19$, $0.7 > p > 0.6$). Surprisingly, as shown in Table S3, the *fer*/+ (Ler × Col-0) plants from the F1 population carried siliques filled to 71.6%, which was significantly higher than the original *fer*/+ plants in the Ler background (65.1%; $\chi^2 = 17.32$, $p < 0.001$). Double-mutant *fer*/+

Figure S1. APM2/AMC Exhibits Low Level of Similarity with PEX13 but Does Not Have a SH3 Domain

(A) Alignment of APM2/AMC amino acid sequence with its orthologous proteins. The alignment was performed with Jellyfish (LabVelocity). Residues conserved across all five sequences are shaded black; residues conserved across three or four sequences are shaded gray. The consensus sequence is shown underneath. The following abbreviations are used: *Arabidopsis thaliana* (NP_187412) (At), *Musa acuminata* (ABC60343) (Ma), *Medicago truncatula* (ABE91475) (Mt), and *Oryza sativa* (NP_001058908 for a and NP_001051486 for b) (Os).

(B) Alignment of APM2/AMC amino acid sequence with PEX13 of *Saccharomyces cerevisiae*. The alignment was performed with Jellyfish (LabVelocity). Residues conserved across both sequences are shaded black. Consensus sequence is shown underneath. The following abbreviations are used: *Arabidopsis thaliana* (NP_187412) (At) and *Saccharomyces cerevisiae* (NP_013292) (Sc). The SH3 domain of *S. cerevisiae* PEX13 is underlined and does not show conservation of critical SH3-domain residues in APM2/AMC (see also Figure S1C).

(C) Alignment of SH3 domains of PEX13 from different organisms [S3] and the corresponding sequence in APM2/AMC [S7]. The alignment was performed with Jellyfish software (LabVelocity). Residues conserved across all four sequences are shaded black; residues conserved across three or two sequences are shaded gray. Arrows indicate the residues involved in SH3-domain ligand binding. The following abbreviations are used: *Saccharomyces cerevisiae* (NP_013292) (Sc), *Pichia pastoris* (AAB09087) (Pp), *Homo sapiens* (NP_002609) (Hs), and *Arabidopsis thaliana* (NP_187412) (At).

(D) Secondary structure prediction of SH3 domains of PEX13 from different organisms [S3] and the SH3-domain sequence proposed for APM2/AMC by Mano et al. [S7]. The program used was SSpro [S6]. The five stranded β barrels of the PEX13 SH3 domains are underlined. Note that the APM2/AMC secondary structure in that region is completely different from any of the other PEX13 SH3 domains. The following abbreviations are used: helix (H), strand (E), and undefined structure (C).

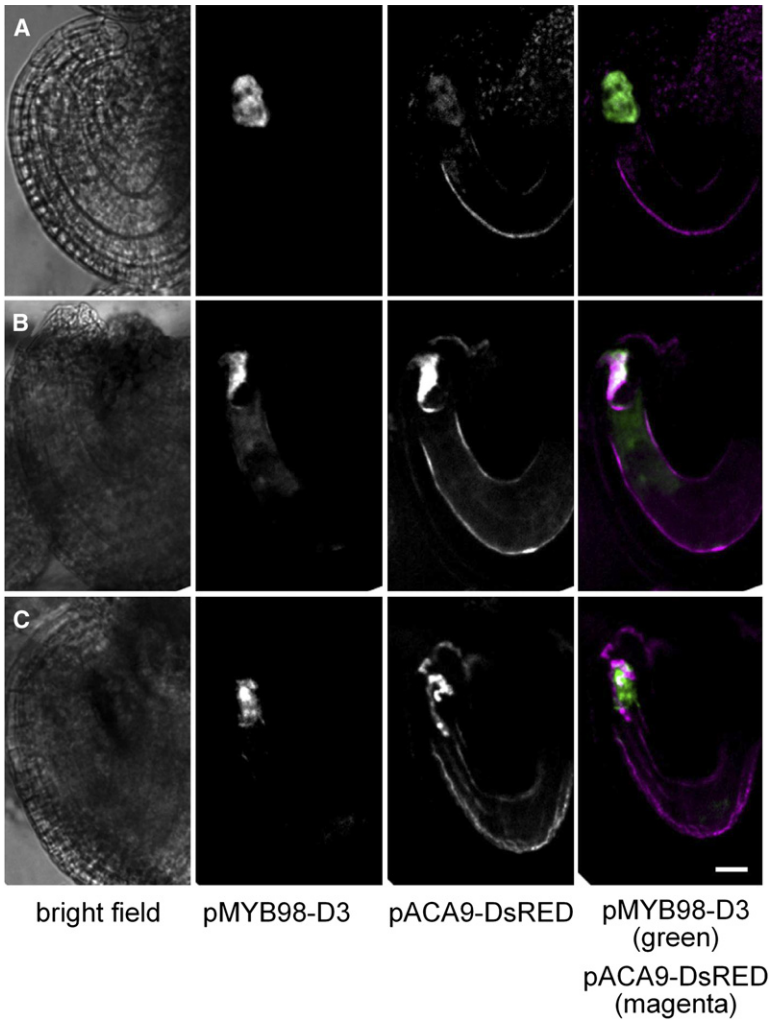

Figure S3. Normal and Delayed Synergid Cell Degeneration during, Respectively, Wild-Type and Mutant Interactions with a Pollen-Tube-Overgrowth Phenotype

Visualization of both synergid cells and pollen tubes before (A) and during fertilization in wild-type (B) and *amc* mutant (C) pollen-ovule interactions. Fluorescence from synergid cells (pMYB98-D3) and pollen tubes (pACA9-DsRED) is observed in green and magenta, respectively. Bright field, pMYB98-D3 (green), and pACA9-DsRED (magenta) are shown in the left, middle-left, and middle-right panels, respectively. The right panels show overlay of green (pMYB98-D3) and magenta (pACA9-DsRED) channels.

(A) Unfertilized mature female gametophytes of *amc*/+ showed normal expression of the synergid cell-specific pMYB98-D3 reporter fusion.

(B) A wild-type pollen-tube discharge (magenta) is associated with a diffused pMYB98-D3 expression (green), indicating normal degeneration of the receptive synergid.

(C) During a mutant *amc* interaction, the pollen tube (magenta) continuously grows around and past the synergid cells that retain a restricted pMYB98-D3 expression (green), indicating the absence of synergid degeneration. The scale bar represents 18 μm.

amc/+ (Ler × Col-0) plants had siliques filled to 67.5%, which was slightly but significantly lower than the seed set of *fer*/+ plants from the same F1 population (71.6%; χ^2 = 7.27, p < 0.01). Although these results should be taken with precaution because of the possible different effects of the ecotype backgrounds on the two mutations, a partial but significant additive effect of the *feronia* and *amc* mutations was observed in the *fer*/+ *amc*/+ double-mutant plants. Therefore, it appears that the two pathways are a least partially independent.

Publicly Available Microarray Data and *APM2/AMC* Promoter Activity in Various Organs

To obtain further insights into the biological function of APM2/AMC in plants, we first analyzed the publicly available ATH1 microarray data from various organs obtained with GENEVESTIGATOR [S10] and from pollen transciptome studies [S11, S12]. *APM2/AMC* was moderately expressed in all organs, with a clear preferential expression in pollen (Figure S4A). In addition, *APM2/AMC* expression levels increased continuously during the course of pollen-grain development (Figure S4A, inset) [S11] to culminate at the mature pollen-grain stage (MPG), correlating with a role for *APM2/AMC* in postpollination functions.

Thirty independent T1 lines expressing the *pAMC-GUS* fusion were generated. Among them, 28 lines exhibited a similar expression pattern and two homozygous single-insertion lines were selected for further analyses. GUS staining was detected throughout young germinating seedlings with the exception of the radicle tips (Figure S4B). One-week-old seedlings exhibited an overall uniform GUS staining (Figure S4C), as did mature leaves (data not shown). GUS levels were strong in young opened flowers, including anthers, filaments, petals, and sepals (Figure S4D). In addition, nondehiscent anther sectioning allowed visualization of *GUS* expression in pollen grains, as well as in the tapetal cell layer surrounding the pollen grains (Figure S4E, white arrows).

APM2/AMC Promoter Activity Is Induced by Pollination

So that the onset of *APM2/AMC* expression in embryo sacs during pollination could be investigated, whole pistils from *pAMC-GUS*-expressing plants were collected and stained 0, 2, 4, 8, and 24 hr after manual self-pollination (Figure S4F). Before pollination (0 hpp), 16.6% (n = 122) of mature female gametophytes exhibited GUS staining. Two and four hours after pollination, as the

pollen tubes started growing in the transmitting tract, the proportion of GUS positive FGs increased to 58.6% (n = 111) and 83.3% (n = 120), respectively. As is clearly depicted in Figure S4F, even unfertilized embryo sacs far away from the front of growing pollen tubes were intensively stained (see also Figure 3C). This indicates that a long-range signal triggered by pollination at the stigma might be able to induce *APM2/AMC* expression in the unfertilized female gametophytes. Interestingly, at 8 and 24 hpp, as fertilization ends and embryo development is initiated, the proportion of GUS-positive embryo sacs dramatically dropped to 18.9% (n = 112) and 11.3% (n = 88), respectively. Therefore, *APM2/AMC* expression in the female gametophyte appears to be transiently induced by pollination and rapidly downregulated after fertilization.

YFP-AMC Fusion Colocalizes with a Peroxisomal Marker in Onion Epidermal Cells

The subcellular localization of APM2/AMC was investigated by transient transformation of onion epidermal cells with a YFP-AMC fusion protein. Although in controls YFP alone was targeted as expected to the cytoplasm and the nucleus (Figure S5A), imaging of the YFP-AMC fusion alone showed a punctuate pattern of expression that is typical for peroxisome-targeted proteins (Figure S5D). To further analyze the localization, we made use of a peroxisomal marker DsRED-KSRM fusion [S13], which alone (Figure S5B) or cobombarded with YFP (Figure S5C) was expressed in onion cell peroxisomes. When YFP-AMC and DsRED-KSRM constructs were cobombarded in onion cells, the YFP signals perfectly merged with the DsRED-derived signals (Figure S5E), indicating that YFP-AMC was indeed localized to peroxisomes.

APM2/AMC Antisense Lines Exhibit Peroxin-Deficient Mutant Phenotypes

Because the *apm2* mutant exhibited only weak peroxin-deficient phenotypes [S7] and the absence of homozygous individuals for the *amc* null mutation prevented us from further elucidating the developmental and cell biological functions of APM2/AMC, antisense lines for *APM2/AMC* were generated with the 35S promoter. This promoter has been shown to drive expression in a wide range of tissues but not in *Arabidopsis* pollen [S14].

Although none of the ten empty-vector control lines showed any obvious phenotype (data not shown), 37 out of the 75 antisense T1 lines exhibited reduced fertility (Figure S6A), which was due to shorter filaments and nondehiscent anthers (data not shown). The antisense lines were also smaller and paler green compared to wild-type plants (Figure S6B). Interestingly, these phenotypes are characteristics of peroxin mutants deficient in photorespiration, a peroxisomal process requiring PTS1-dependent import [S15–S18]. Quantitative real-time PCR analysis confirmed that *APM2/AMC* expression was efficiently reduced in the small, pale green antisense lines (Figure S6C). Thus, these novel findings suggest that APM2/AMC is required for proper peroxisomal photorespiration.

So that the effect of reduced expression levels of *APM2/AMC* on PTS1-dependent import of proteins could be directly investigated, the antisense line 2 (AS2) was crossed with plants expressing GFP-PTS1 (GFP: green fluorescent protein) fusion protein [S19]. In intact wild-type leaves expressing the GFP-PTS1 fusion, as expected, GFP fluorescence showed a punctuate pattern of expression consistent with peroxisomal localization (Figure S6D). Although some peroxisomes still exhibited fluorescence from the GFP-PTS1 fusion in the antisense line, most of the fluorescence shifted from peroxisomes to the cytosol (Figure S6E), and this was particularly evident in guard cells (Figure S6E, insets). Thus, the presence of abundant GFP-PTS1 fluorescence in the cytoplasm of the antisense line indicated a decrease of the efficiency of PTS1-dependent protein import into peroxisomes. Together, our results indicate that APM2/AMC functions in vegetative tissues as a peroxin that participates in the PTS1-import pathway.

The *amc* Mutation Affects Neither Pollen Germination nor Pollen-Tube Growth In Vitro

Because the pollen peroxisome targeting pLAT52-CFP-PTS1 construct allowed us to directly differentiate wild-type pollen tubes (fluorescence in the peroxisomes) from the *amc* mutant PTs (fluorescence in the cytosol) within an *amc*/+ pollen tetrad (see Results and Discussion), *amc*/+ plants homozygous for the pLAT52-CFP-PTS1 construct were recovered to perform pollen germination and pollen-tube growth in vitro [S20, S21]. After 6 hr of incubation in vitro, the germination rate of *amc* pollen grains (45.4%, n = 109 out of 240) was similar to the one of wild-type grains (51.2%, n = 123 out of 240), and, as illustrated in Figure S7, *amc* PTs grew as well as wild-type PTs (*amc*, 115.2 ± 55.2 μm, n = 219, arrowheads; WT, 101.5 ± 36.7 μm, n = 229, arrows). These results indicate that in vitro pollen germination and pollen-tube growth are not affected by the *amc* mutation.

Supplemental Experimental Procedures

Plant Growth Conditions and Morphological Analyses of Mutant Siliques

Arabidopsis thaliana plants (ecotype Columbia 0) were grown in a Conviron growth chamber (Winnipeg, Canada) in plastic pots filled with ready-to-use soil (Professional Blend [Sunshine, Canada]). After the sewing, pots were kept at 4°C for 2–4 days. Growing conditions were 19°C –22°C, 75% humidity, with a 16 hr light/8 hr dark photoperiod regime at ~95 $\mu E.m^{-2}.s^{-1}$. For manual crosses, closed flower buds from late stage 12 according to Smyth et al. [S22] were emasculated and then manually pollinated 24 hr later with dehiscent anthers from pollen-donor flowers under a dissecting microscope. For morphological analysis, ovules from dissected siliques were mounted in Hoyer's medium and imaged with a Leica DM5000B compound microscope under Nomarski optics. Aniline blue staining was performed as described previously [S23], and samples were examined and photographed with a Leica TCS SP2 confocal microscope (Leica Microsystems [Germany]; 405 nm excitation and 405–480 nm emission).

Mutant-Line Genotyping

The *amc* allele of the At3g07560 gene was obtained from the Signal Collection at the Salk Institute (La Jolla, California) [S24] and corresponds to the Salk_055083 line. Genotyping PCR reactions for mutants were performed with a combination of primers b and c (5′-GGCAGTCCTCCTAAACCTTGGG-3′ and 5′-CCATCGCACCACC ACCATACATGCC-3′), b and LBa1 (5′-TGGTTCACGTAGTGGGCCA TCG-3) and finally c and RBa1 (5′-GCTCATTAAACTCCAGAA ACCCGCG-3′), and amplified products were sequenced (Figure 1C). *feronia*/+ (Landsberg ecotype) seeds were kindly provided by Ueli

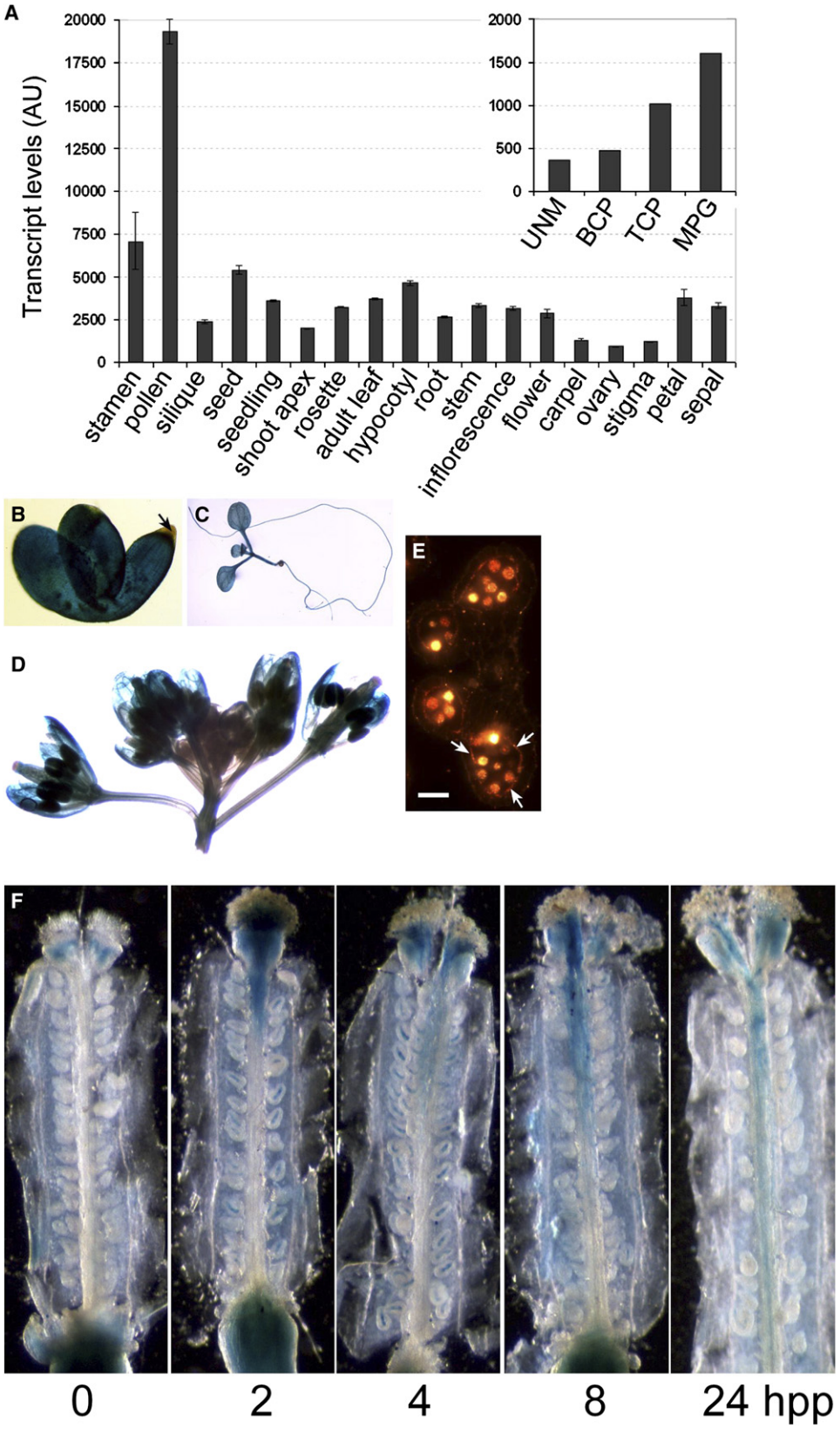

Figure S4. Publicly Available Microarray Data and *APM2/AMC* Promoter Activity in *Arabidopsis*

(A) Microarray data for *APM2/AMC* in different organs retrieved from GENEVESTIGATOR [S10] (downloaded April 2006) ± the standard error. Transcript levels for *APM2/AMC* were detected in every tissue with the highest expression in pollen. The inset shows microarray data retrieved from Honys and Twell [S11] showing a constant increase of *APM2/AMC* transcript levels during the course of pollen development. The following abbreviations are used: uninucleate microspores (UNM), bicellular pollen (BCP), immature tricellular pollen (TCP), and mature pollen grain (MPG).

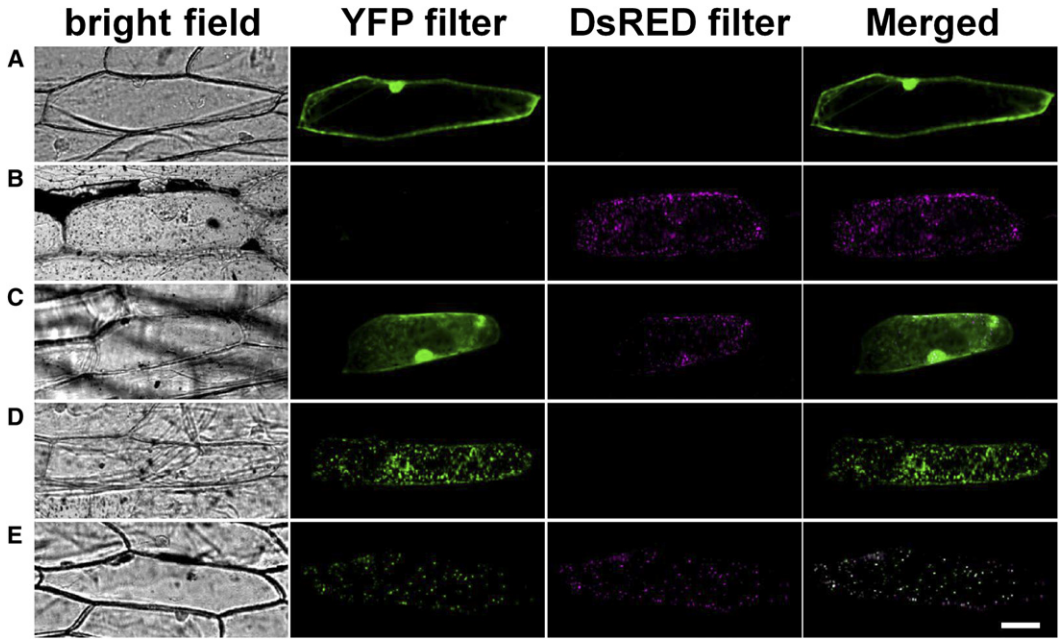

Figure S5. The YFP-AMC and DsRED-KSRM Fusions Colocalize in Peroxisomes

Plasmids encoding YFP, YFP-AMC, and the peroxisomal DsRED-KSRM marker were independently or coexpressed in onion epidermal cells by particle bombardment. Filters are indicated on the top.

(A) YFP alone.

(B) DsRED-KSRM alone.

(C) YFP and DsRED-KSRM.

(D) YFP-AMC alone.

(E) YFP-AMC and DsRED-KSRM colocalized in peroxisomes. The scale bar represents 65 μm.

Grossniklaus (Institute of Plant Biology [Zurich, Switzerland]) and genotyped as previously described [S9].

Constructs and Generation of Transgenic Plants

We introduced the binary vectors constructed and described below into *Agrobacterium tumefaciens* strain GV3101 by electroporation, which we then used to transform by floral dipping [S25] wild-type or Kanamycin-resistant *amc*/+ plants in a *quartet* mutant background [S26–S28].

For *amc*/+ genomic complementation, a KpnI/ClaI 4432 bp long fragment was recovered from digestion of the F21O3 BAC and cloned into the KpnI/ClaI cut binary pGreenII-0229 vector [S29] conferring resistance to Basta. To identify *amc*/*amc* homozygous individuals among the progeny of the complemented line, we used the combination of primers b and LBa1 to amplify the T-DNA specific band and the combination of primers c and a (5′-CCGAAACACTT ATGCTCCTTCTAATCC-3′) located outside of the 4.4 Kb BAC genomic construct to amplify the wild-type genomic band (see Figure 1C).

pACA9-DsRED as well as pACA9-D3 (the cameleon reporter containing the YFP) [S30] and pMYB98-D3 constructs were generated and kindly provided by Jeffrey Harper (Biochemistry Department, University of Nevada, Reno [Nevada]).

For the *APM2*/*AMC* gene promoter *GUS* reporter fusion, a 1392 bp fragment of the *APM2*/*AMC* locus was PCR amplified from the F21O3 BAC with 5′-ACTAATCAATAAAGCTTATACACGAAGAAGG-3′ and 5′-GCTAACCTGCAGGATCCGACGCCATATATC-3′ primers introducing the HindIII and BamHI sites (underlined), respectively, and cloned into pGEM-T Easy vector (Promega, [Madison, Wisconsin]) and sequenced. The 1392 bp fragment was then subcloned into the binary plant vector pLP100 [S31] for the generation of a precise transcriptional fusion with the *gusA* reporter gene with HindIII and BamHI sites.

The pLAT52-CFP-PTS1 fusion in a pBluescript SKII vector [S32] was kindly provided by Ana Silva and José Feijó (Fundação Calouste Gulbenkian, Instituto Gulbenkian de Ciência [Lisboa, Portugal]). pLAT52-CFP-PTS1 was extracted by a KpnI/SacI digestion and then cloned into the KpnI/SacI cut binary pGreenII-0179 vector [S29] conferring resistance to Hygromycin.

Microscopic Phenotyping of Wild-Type and *amc/+* Mutant Pollen-Ovule Interactions

For YFP- or DsRED-expressing pollen and YFP-expressing synergid cell observations, 19 to 24 hr after manual pollination, pistils were glued to a slide and cut along the replum with a micro knife (Fine Science Tools [Foster City, California]) under a dissecting microscope. The valves were carefully removed so that only the stigma and the septum with the attached ovules glued to the slide were submerged in 20% glycerol. Fluorescence imaging was acquired by spinning-disc confocal microscopy with a QLC100 confocal-scanning unit (Solamere Technology Group [Salt Lake City, Utah]) linked to a NIKON Eclipse TE 2000-U bright-field microscope (Tokyo, Japan) and an argon laser (500 M Select, Laserphysics [West Jordan, Utah]). Images were captured with an electron-multiplying

(B–F) Histochemical localization of *GUS* reporter gene expression driven by the *APM2*/*AMC* promoter in different organs or tissues of *Arabidopsis* (B–E) and during pollination (F). (B) shows a germinating seedling; note that staining is absent from the radicle tip (arrow). (C) shows a one week-old seedling. (D) shows inflorescence. (E) shows a dark-field photograph of a nondehiscent anther section showing staining in pollen grains as well as in the surrounding tapetum (arrows). The scale bar represents 300 μm. GUS activity in the embryo sacs is induced by pollination to culminate 4 hr after pollination but decreases after fertilization (F).

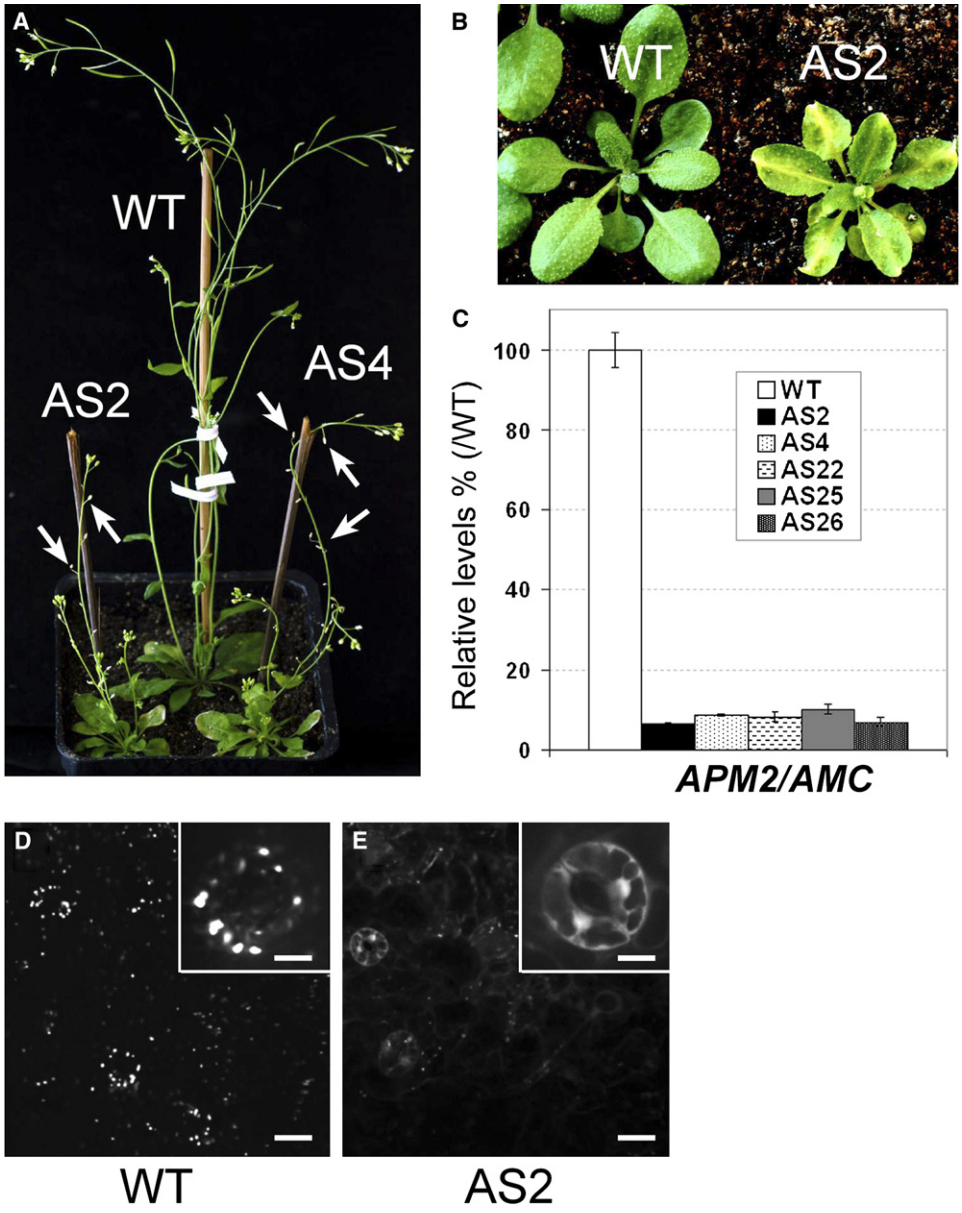

Figure S6. Peroxin-Deficient Phenotypes Related to Photorespiration and PTS1-Dependent Protein Import into Peroxisomes of the *APM2/AMC* Antisense Lines

(A) Six-week-old wild-type plant (WT) and *APM2/AMC* antisense lines (AS2 and AS4) grown at 24°C. The *APM2/AMC* antisense plants were partially sterile, with dried flowers (arrows) instead of developing siliques.

(B) Four-week-old plants. *APM2/AMC* antisense lines (AS2, right) were smaller and paler green compared to the wild-type (WT, left).

(C) Quantitative real-time RT-PCR analysis indicates that *APM2/AMC* transcript levels are reduced to approximately 7%–11% of wild-type levels in five independent *APM2/AMC* antisense lines (AS2, 4, 22, 25, 26). Each data point indicates the average of three independent experiments ± SEM

(D and E) GFP fluorescence from intact leaves of GFP-PTS1 expressing wild-type (D) and AMCantisense line 2 (E) plants. Scale bars represent 21 μM in (D) and (E). The insets in (D) and (E) show enlarged views of the corresponding guard cells. Scale bars represent 7 μM in the insets.

charge-coupled device (EMCCD) camera (Cascade II:512, Photometrics [Tucson, Arizona]) with Metamorph software (Universal Imaging [Downington, Pennsylvania]). For YFP observation, laser excitation was 488 nm, and YFP fluorescence was selected in the green channel with a band-pass 500–550 nm filter. For DsRED or autofluorescence, laser excitation was 568 nm, and fluorescence was selected in the red channel (converted to magenta) with a band-pass 580–650 nm filter. Z stacks with 0.5 to 1 μm intervals were recorded for each channel, processed with the Metamorph stack arithmetic "best focus" function, and then overlaid.

Gene-Expression Analyses

Total RNA was extracted from vegetative tissues of 2-week-old plants and from inflorescences and pollen of mature plants with Trizol reagent (Life Technologies, GIBCO-BRL [Rockville, Maryland]). After DNase I treatment (DNA-*free*, Ambion [Austin, Texas]), reverse transcription (First-strand cDNA Synthesis Kit, Amersham Biosciences [Piscataway, New Jersey]) was performed on 2.5 μg RNA, and 2 μl was used for PCR reactions. Samples were withdrawn after 23, 27, 31, and 35 cycles, and products were analyzed by agarose gel electrophoresis. Primers used for *ACTIN7* (At5g09810) were

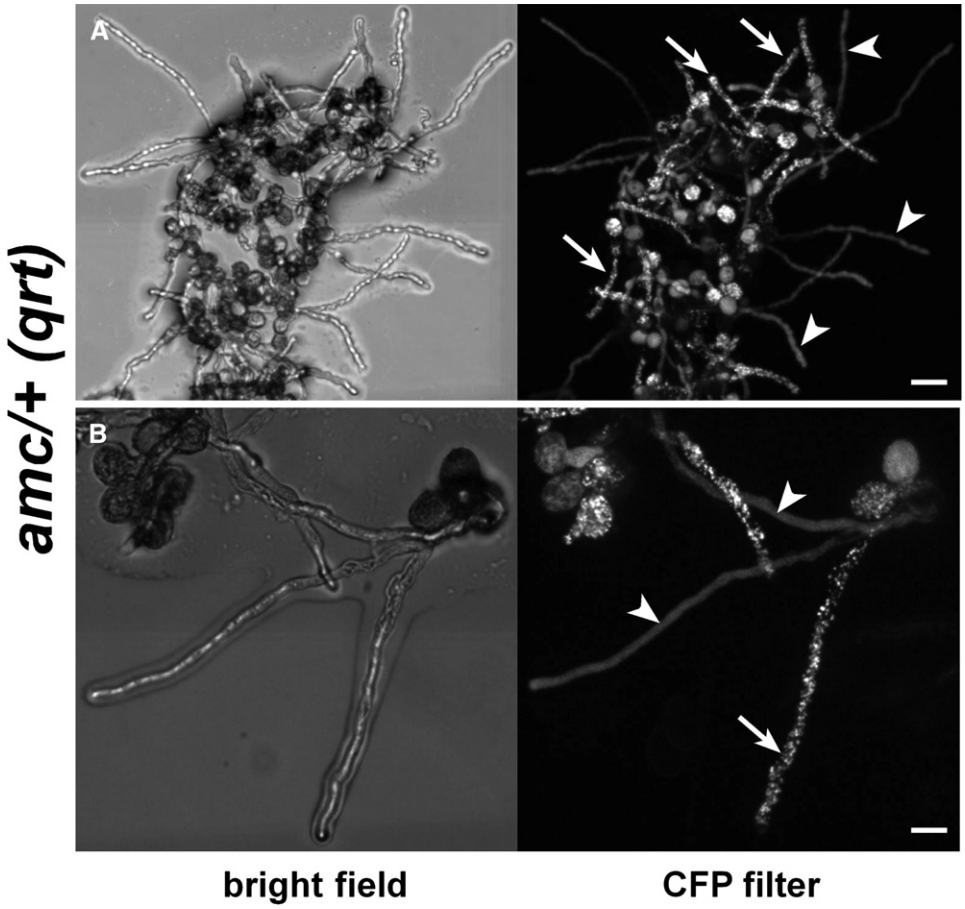

Figure S7. *amc* Mutant Pollen Germinates and Grows In Vitro as well as Wild-Type Pollen

Within tetrads from *amc*/+ (*qrt*) plants homozygous for the peroxisomal pLAT52-CFP-PTS1 marker, mutant *amc* pollen (fluorescence in the cytosol, arrowheads) germinated and grew as well as wild-type pollen (fluorescence in peroxisomes, arrows). Scale bars represent 45 μm and 25 μm for (A) and (B), respectively.

5′-GGCCGATGGTGAGGATATTCAGCCACTTG-3′ and 5′-TCGATGGACCTGACTCATCGTACTCACTC-3′ and for *APM2/AMC* (At3g07560) were 5′-GTTACTTCTTTCATTACCCAAATCC-3′ and 5′-TCAATAGAAAGGTCTTTAACAAACAC-3′.

For quantitative real-time PCR, the complementary DNAs (cDNAs) obtained from above were diluted five times. Then, quantitative PCR was performed with a LightCycler (Roche) with the SYBR Green I detection system, under the following conditions: 95°C for 10 min, 45 cycles of 95°C for 5 s, 58°C for 5 s, and 72°C for 13 s, followed by melting curve analysis. Primers used for *Clathrin* (At4g24550) were 5′-ATACGCGCTGAGTTCCCG-3′ and 5′-CTGACTGGCCCTGCTT-3′. PCR mixture of a final volume of 10 μl contained 2 μl of cDNA, 0.5 μM of each primer, 4 mM Mg^{2+}, and 1 μL of LightCycler-FastStart DNA Master SYBR Green I mixture (Roche). Quantitative data analyses were performed with the LightCycler software 4.0 (Roche).

Histochemical GUS assays were performed essentially as described before [S33] with a GUS substrate solution containing 1 mM 5-bromo-4-chloro-3-indolyl-β-D-glucuronic acid (X-Gluc), 0.1 M sodium phosphate buffer (pH 7.0), 0.1% Triton X-100, 0.5 mM $K_3[Fe(CN)_6]$, 0.5 mM $K_4[Fe(CN)_6]$, and 5 mM thylenediaminetetraacetic acid (EDTA). Incubation was performed in the dark at 37°C for periods of time between 1 and 14 hr, depending upon the intensity of the staining. For cross-sections, inflorescences were then fixed in FAA (35% paraformaldehyde/glacial acetic acid/70% ethanol [1:1:9, v/v/v]) for 4 hr then dehydrated with increasing ethanol solutions. Ethanol was progressively replaced by Histoclear II (National Diagnostics [Atlanta, Georgia]) and Histoclear II by Paraplast Embedding Media (Sigma [St Louis, Missouri]). Eight μm sections were then mounted in Permount (Fisher Scientific [Hampton, New Hampshire]).

Table S1. Segregation Analysis of the *amc* Mutation Using the Kanamycin Marker

Female × Male	Kan^S	Kan^R	% Kan^R	% TE
amc/+ × *amc*/+	740	1233	62.5	nd
amc/+ × +/+	166	151	47.6	91
+/+ × *amc*/+	283	154	35.2	54.4

"nd" indicates not determined.

Generation of *APM2/AMC* Antisense Lines and GFP-PTS1 Fluorescence Imaging

For the generation of the *APM2/AMC* antisense lines, the full-length *APM2/AMC* cDNA was PCR amplified with 5′-GCGGCCGCATGGCGTCTCAGCCTGCAGG-3′ (introducing a NotI site, underlined) and 5′-CCCGGGTTAGTTGCCCCATACATTGTCC-3′ (introducing a SmaI site, underlined). The cDNA was cloned into pGEM-T Easy (Promega [Madison, Wisconsin]), sequenced, and then cloned into the SmaI/NotI cut binary 35SpBARN vector (conferring Basta resistance) [S34].

A GFP-PTS1-expressing line in the Col-0 background [S19] was kindly provided by Shoji Mano and Mikio Nishimura (Department of Cell Biology, National Institute for Basic Biology [Okazaki, Japan]). Pistils from GFP-PTS1 line were pollinated with pollen from *APM2/AMC* antisense line 2 (Basta resistant). Intact leaves from F1 Basta-resistant seedlings as well as from the parental GFP-PTS1

Table S2. Expected and Observed Class Frequencies within the Progeny of Selfed *amc*/+ Plants, Based on Table 1

Classes	Pollen Frequency	Ovule Frequency	Expected Class Frequency if *amc*/*amc* Exists	Expected Class Frequency if *amc*/*amc* Is Missing	Observed Class Frequency
amc/*amc*	0.337 (*amc*)	0.453 (*amc*)	0.153	0	0
amc/+	0.337 (*amc*), 0.663 (+)	0.547 (+), 0.453 (*amc*)	0.184 + 0.3 = 0.484	0.571	0.584
+/+	0.663 (+)	0.547 (+)	0.363	0.429	0.416

line were then examined by confocal laser-scanning microscopy (CLSM) with the same setup as for the observations of the YFP-expressing pollen.

Transient Expression in Onion Epidermal Cells

For the YFP-AMC construct, the full-length *APM2*/*AMC* cDNA was PCR amplified with 5′-CTTAGATCTATGGCGTCTCAGCCTGCA GGT-3′ (introducing a BglII site, underlined) and 5′-AGATCTAGATTA GTTGCCCCATACATTGTC-3′ (introducing a XbaI site, underlined), digested, and cloned into a YFP-tagging vector (35S:YFP, GenBank accession number AY189981) [S35] cut with BglII and XbaI, followed by sequencing. The pRTL2-DsRED-KSRM plasmid was kindly provided by Ning-Hui Chen (Baylor College of Medicine [Houston, Texas]).

Plasmids encoding the YFP-AMC, DsRED-KSRM, and YFP alone were independently or coexpressed in onion epidermal cells by particle bombardment (PDS-1000/He, Bio-Rad) as described previously [S36]. After 1 day of incubation, transient gene expressions were examined by confocal microscopy (same experimental setup as for the observations of the YFP-expressing pollen). For YFP observations, a 488 nm laser excitation was coupled with a band-pass 500–550 nm filter (green channel), whereas for DsRED, excitation was 568 nm coupled with a band-pass 580–650 nm filter (red channel, converted to magenta).

CFP-PTS1 Fluorescence Imaging in Pollen

Pollen tetrads of wild-type and *amc*/+ T1 Hygromycin-resistant plants expressing the pLAT52-CFP-PTS1 fusion were deposited on slides and submerged in 20% glycerol. Fluorescent pollen grains from the tetrads were then counted and examined by CLSM with the same setup as for the observations of the YFP-expressing pollen, except laser excitation was 440 nm and fluorescence was selected with a band-pass 440–514 nm filter. In vitro pollen-germination and pollen-tube-growth assays (Supplemental Results and Discussion and Figure S7) were carried out as previously described [S20, S21].

Supplemental References

S1. Gasteiger, E., Gattiker, A., Hoogland, C., Ivanyi, I., Appel, R.D., and Bairoch, A. (2003). ExPASy: The proteomics server for in-depth protein knowledge and analysis. Nucleic Acids Res. *31*, 3784–3788.

S2. Mayer, B.J. (2001). SH3 domains: Complexity in moderation. J. Cell Sci. *114*, 1253–1263.

S3. Williams, C., and Distel, B. (2006). Pex13p: Docking or cargo handling protein? Biochim. Biophys. Acta *1763*, 1585–1591.

S4. de Castro, E., Sigrist, C.J., Gattiker, A., Bulliard, V., Langendijk-Genevaux, P.S., Gasteiger, E., Bairoch, A., and Hulo, N. (2006). ScanProsite: Detection of PROSITE signature matches and ProRule-associated functional and structural residues in proteins. Nucleic Acids Res. *34*, W362–W365.

S5. Finn, R.D., Mistry, J., Schuster-Bockler, B., Griffiths-Jones, S., Hollich, V., Lassmann, T., Moxon, S., Marshall, M., Khanna, A., Durbin, R., et al. (2006). Pfam: Clans, web tools and services. Nucleic Acids Res. *34*, D247–D251.

S6. Pollastri, G., Przybylski, D., Rost, B., and Baldi, P. (2002). Improving the prediction of protein secondary structure in three and eight classes using recurrent neural networks and profiles. Proteins *47*, 228–235.

S7. Mano, S., Nakamori, C., Nito, K., Kondo, M., and Nishimura, M. (2006). The *Arabidopsis pex12* and *pex13* mutants are defective in both PTS1- and PTS2-dependent protein transport to peroxisomes. Plant J. *47*, 604–618.

S8. Kasahara, R.D., Portereiko, M.F., Sandaklie-Nikolova, L., Rabiger, D.S., and Drews, G.N. (2005). MYB98 is required for pollen tube guidance and synergid cell differentiation in *Arabidopsis*. Plant Cell *17*, 2981–2992.

S9. Escobar-Restrepo, J.M., Huck, N., Kessler, S., Gagliardini, V., Gheyselinck, J., Yang, W.C., and Grossniklaus, U. (2007). The FERONIA receptor-like kinase mediates male-female interactions during pollen tube reception. Science *317*, 656–660.

S10. Zimmermann, P., Hirsch-Hoffmann, M., Hennig, L., and Gruissem, W. (2004). GENEVESTIGATOR. *Arabidopsis* microarray database and analysis toolbox. Plant Physiol. *136*, 2621–2632.

S11. Honys, D., and Twell, D. (2004). Transcriptome analysis of haploid male gametophyte development in *Arabidopsis*. Genome Biol. *5*, R85.

S12. Pina, C., Pinto, F., Feijo, J.A., and Becker, J.D. (2005). Gene family analysis of the *Arabidopsis* pollen transcriptome reveals biological implications for cell growth, division control, and gene expression regulation. Plant Physiol. *138*, 744–756.

S13. Trelease, R.N., Lee, M.S., Banjoko, A., and Bunkelmann, J. (1996). C-terminal polypeptides are necessary and sufficient for *in vivo* targeting of transiently-expressed proteins to peroxisomes in suspension-cultured plant cells. Protoplasma *195*, 156–167.

S14. Wilkinson, J.E., Twell, D., and Lindsey, K. (1997). Activities of CaMV 35S and *nos* promoters in pollen: Implications for field release of transgenic plants. J. Exp. Bot. *48*, 265–275.

S15. Hayashi, M., Nito, K., Toriyama-Kato, K., Kondo, M., Yamaya, T., and Nishimura, M. (2000). AtPex14p maintains peroxisomal functions by determining protein targeting to three kinds of plant peroxisomes. EMBO J. *19*, 5701–5710.

S16. Zolman, B.K., and Bartel, B. (2004). An *Arabidopsis* indole-3-butyric acid-response mutant defective in PEROXIN6, an apparent ATPase implicated in peroxisomal function. Proc. Natl. Acad. Sci. USA *101*, 1786–1791.

Table S3. Seed Set of Siliques from Self-Pollinated *fer*/+ or *amc*/+ Single Mutants and the F1 Plants Resulting from a *fer*/+ × *amc*/+ Cross

Genotype	Percent of Nonaborted Ovules in Siliques	Different Categories Based on Chi-Square Test
amc/+ (Col-0)	76 (n = 891)	a
fer/+ (Ler)	65.1 (n = 395)	b
F1 Plants from *fer*/+ (Ler) × *amc*/+ (Col-0)		
amc/+	77.3 (n = 209)	a
fer/+	71.6 (n = 933)	c
fer/+ *amc*/+	67.5 (n = 926)	b

S17. Fan, J., Quan, S., Orth, T., Awai, C., Chory, J., and Hu, J. (2005). The *Arabidopsis PEX12* gene is required for peroxisome biogenesis and is essential for development. Plant Physiol. *139*, 231–239.

S18. Hayashi, M., Yagi, M., Nito, K., Kamada, T., and Nishimura, M. (2005). Differential contribution of two peroxisomal protein receptors to the maintenance of peroxisomal functions in *Arabidopsis*. J. Biol. Chem. *280*, 14829–14835.

S19. Mano, S., Nakamori, C., Hayashi, M., Kato, A., Kondo, M., and Nishimura, M. (2002). Distribution and characterization of peroxisomes in *Arabidopsis* by visualization with GFP: Dynamic morphology and actin-dependent movement. Plant Cell Physiol. *43*, 331–341.

S20. Fan, L.M., Wang, Y.F., Wang, H., and Wu, W.H. (2001). *In vitro Arabidopsis* pollen germination and characterization of the inward potassium currents in *Arabidopsis* pollen grain protoplasts. J. Exp. Bot. *52*, 1603–1614.

S21. Frietsch, S., Wang, Y.F., Sladek, C., Poulsen, L.R., Romanowsky, S.M., Schroeder, J.I., and Harper, J.F. (2007). A cyclic nucleotide-gated channel is essential for polarized tip growth of pollen. Proc. Natl. Acad. Sci. USA *104*, 14531–14536.

S22. Smyth, D.R., Bowman, J.L., and Meyerowitz, E.M. (1990). Early flower development in *Arabidopsis*. Plant Cell *2*, 755–767.

S23. Schiott, M., Romanowsky, S.M., Baekgaard, L., Jakobsen, M.K., Palmgren, M.G., and Harper, J.F. (2004). A plant plasma membrane Ca2+ pump is required for normal pollen tube growth and fertilization. Proc. Natl. Acad. Sci. USA *101*, 9502–9507.

S24. Alonso, J.M., Stepanova, A.N., Leisse, T.J., Kim, C.J., Chen, H., Shinn, P., Stevenson, D.K., Zimmerman, J., Barajas, P., Cheuk, R., et al. (2003). Genome-wide insertional mutagenesis of *Arabidopsis thaliana*. Science *301*, 653–657.

S25. Clough, S.J., and Bent, A.F. (1998). Floral dip: A simplified method for *Agrobacterium*-mediated transformation of *Arabidopsis thaliana*. Plant J. *16*, 735–743.

S26. Preuss, D., Rhee, S.Y., and Davis, R.W. (1994). Tetrad analysis possible in *Arabidopsis* with mutation of the *QUARTET* (*QRT*) genes. Science *264*, 1458–1460.

S27. Copenhaver, G.P., Keith, K.C., and Preuss, D. (2000). Tetrad analysis in higher plants. A budding technology. Plant Physiol. *124*, 7–16.

S28. Johnson-Brousseau, S.A., and McCormick, S. (2004). A compendium of methods useful for characterizing *Arabidopsis* pollen mutants and gametophytically-expressed genes. Plant J. *39*, 761–775.

S29. Hellens, R.P., Edwards, E.A., Leyland, N.R., Bean, S., and Mullineaux, P.M. (2000). pGreen: A versatile and flexible binary Ti vector for *Agrobacterium*-mediated plant transformation. Plant Mol. Biol. *42*, 819–832.

S30. Palmer, A.E., Giacomello, M., Kortemme, T., Hires, S.A., Lev-Ram, V., Baker, D., and Tsien, R.Y. (2006). Ca2+ indicators based on computationally redesigned calmodulin-peptide pairs. Chem. Biol. *13*, 521–530.

S31. Szabados, L., Charrier, B., Kondorosi, A., Debruijn, F.J., and Ratet, P. (1995). New plant promoter and enhancer testing vectors. Mol. Breed. *1*, 419–423.

S32. Prado, A.M., Porterfield, D.M., and Feijo, J.A. (2004). Nitric oxide is involved in growth regulation and re-orientation of pollen tubes. Development *131*, 2707–2714.

S33. Boisson-Dernier, A., Andriankaja, A., Chabaud, M., Niebel, A., Journet, E.P., Barker, D.G., and de Carvalho-Niebel, F. (2005). *MtENOD11* gene activation during rhizobial infection and mycorrhizal arbuscule development requires a common AT-rich-containing regulatory sequence. Mol. Plant Microbe Interact. *18*, 1269–1276.

S34. LeClere, S., and Bartel, B. (2001). A library of *Arabidopsis* 35S-cDNA lines for identifying novel mutants. Plant Mol. Biol. *46*, 695–703.

S35. Subramanian, C., Kim, B.H., Lyssenko, N.N., Xu, X., Johnson, C.H., and von Arnim, A.G. (2004). The *Arabidopsis* repressor of light signaling, COP1, is regulated by nuclear exclusion: mutational analysis by bioluminescence resonance energy transfer. Proc. Natl. Acad. Sci. USA *101*, 6798–6802.

S36. von Arnim, A.G., Deng, X.W., and Stacey, M.G. (1998). Cloning vectors for the expression of green fluorescent protein fusion proteins in transgenic plants. Gene *221*, 35–43.